JOURNAL OF GEOPHYSICAL RESEARCH, VOL. 100, NO. C7, PAGES 13,655–13,663, JULY 15, 1995

Path-averaged measurements of turbulence beneath ice in the Arctic

Dimitris Menemenlis

Earth, Atmospheric and Planetary Sciences, Massachusetts Institute of Technology, Cambridge

David M. Farmer

Ocean Physics, Institute of Ocean Sciences, Sidney, British Columbia, Canada

Abstract. Two-way acoustic propagation measurements obtained along 200-m horizontal paths, a few meters below ice in the eastern Arctic, are used to estimate energy dissipation rate and momentum transfer between the ice and the ocean. Forward scattered sound propagating through the turbulent fluid of the boundary layer under ice produces characteristic scintillation patterns at the receivers which are interpreted in terms of the refractive index fine structure of the flow. Reciprocal travel time measurements yield information about the velocity variability along each acoustic path. By combining these two types of measurements, the contributions of sound speed and water-particle velocity fluctuations to forward acoustic scatter can be separated. For the particular case of the under-ice boundary layer, sound speed variability is negligible. Therefore, under the assumptions of a Kolmogorov inertial subrange and Taylor's frozen field hypothesis, the one-way and the reciprocal acoustical measurements provide two independent estimates of turbulent kinetic energy dissipation rate averaged over the propagation paths. Both these methods yield a value of 8×10^{-8} W kg^{-1} 6 m from the bottom of the ice for a 7-hour period during which the mean ice–relative velocity is 0.11 m s^{-1}. Surface layer approximations then yield a value of 0.03 N m^{-2} for turbulent stress near the surface. The acoustical measurements also indicate that circulation around ice keels can cause horizontal "lift forces" of order 10^4 N.

Introduction

In order to model the interaction between the polar oceans and the atmosphere and predict the extent and drift of the ice cover, it is necessary to measure and describe small-scale processes that occur in a turbulent boundary layer just beneath the ice. Measurements in this layer have traditionally been carried out using instruments that have a high degree of spatial resolution [*Langleben*, 1982; *Shirasawa*, 1986; *McPhee*, 1990; *Padman and Dillon*, 1991]. The drawback to these methods is that they are essentially local in character and can therefore be biased by local flow inhomogeneities due to the irregular ice topography and the intermittency of dissipation events. Here we describe a reciprocal acoustic propagation experiment which provided horizontally integrated properties of the turbulent flow along 200-m horizontal paths a few meters beneath ice. These measurements are compared with concurrent in situ observations.

Paper number 95JC01252.
0148-0227/95/95JC-01252$05.00

Point measurements can sense individual turbulent eddies, but the statistical description of a turbulent flow is more useful for oceanographic purposes. For this reason, Taylor's frozen field hypothesis is invoked to estimate streamwise correlation functions from single-point time series [e.g., *Lumley and Panofsky*, 1964, section 1.17]. This hypothesis is the approximation that the turbulence is essentially frozen as it is advected past the instrument. It is valid when the kinetic energy of the fluctuations is much smaller than that of the mean ice–relative flow. When this approximation holds, space correlation functions or wavenumber spectra can be inferred from the time series.

However, these statistical estimates must be interpreted with care. *McPhee* [1990] cites an example in which surface stress calculated from simultaneous current meter profiles, spaced about 100 m apart, varied by a factor of 2.5 due to local under-ice topography. In addition to localized flow inhomogeneity, geophysical turbulence is a patchy and intermittent process. *Oakey and Elliott* [1982] observed significant changes, often a factor of 10, in turbulence levels between two profiles a few minutes apart. *Yamazaki et al.* [1990] report a factor of 2 difference between vertical and horizontal measurements of dissipation rates. These differences emphasize the necessity of adequate space-time averag-

ing to obtain representative estimates of the statistical properties of turbulent flows.

The advantage of the acoustical techniques described in this paper is that they acquire path-averaged properties over baselines several times that of the turbulent eddies being measured. Forward scattered sound provides the basis for probing the sound speed fine structure of turbulent flows [*Flatté*, 1983; *Farmer et al.*, 1987; *DiIorio and Farmer*, 1994]. Reciprocal travel time measurements contain information about the velocity fine structure [*Menemenlis*, 1993, 1994]. These remote sensing techniques forfeit the observation of individual eddies in favor of a more representative statistical description of the turbulence.

Here these methods are applied to acoustical measurements that were collected by *Menemenlis and Farmer* [1992] as part of the Coordinated Eastern Arctic Experiment (CEAREX). The resulting statistical information about the sound speed and water-particle velocity fine structure of the mixed layer is used to estimate turbulent kinetic energy dissipation rate, momentum transfer between the ice and the ocean, and the drag coefficient.

In addition, the particular configuration of the acoustical array allows a direct measurement of circulation around the ice keels enclosed by the acoustic paths. This signal is used to estimate the horizontal "lift forces" exerted on the keels by the mean flow.

Theory

The purpose of this section is to introduce the notation and the equations required for studying under-ice turbulence using the acoustical measurements. Theoretical results will be stated without derivation as more complete discussions are to be found in the references. We first consider the use of acoustical amplitude fluctuations at the receiving hydrophone to infer the statistical properties of the intervening turbulent flow. Next we discuss the interpretation of fluctuations in reciprocal travel time difference. It is shown that under certain circumstances these two signals can be used to estimate kinetic energy dissipation rate ε. We also review how ε can be used to approximate the drag coefficient and the stress exerted by the ocean on the ice. The reader who is primarily interested by the experimental results may skip this section at first reading.

Forward Scattered Sound

The theory of wave propagation through random media is well developed for the weak scattering regime [*Lee and Harp*, 1969; *Tatarskii*, 1971; *Ostashev*, 1994]. *Tatarskii* [1993] gives a particularly cogent qualitative interpretation. Briefly, the refractive index inhomogeneities of the flow act as weak lenses which focus or disperse the incoming acoustic energy. This effect is responsible for the so-called "scintillation" of the acoustic amplitude at the receiving hydrophone, in the same way that light from distant stars appears to scintillate because it interacts with the turbulent atmosphere. For geometrical optics the largest focusing effect is caused by the smallest lenses because of their smaller radii of curvature and focal lengths. However, owing to diffraction effects, lenses with dimensions smaller than the first Fresnel zone size, $(\lambda_a \ell)^{1/2}$, cannot focus or defocus the acoustic energy. Therefore the most effective scatterers are turbulent scales in the neighborhood of $(\lambda_a \ell)^{1/2}$, where λ_a is the acoustic wavelength and ℓ is the range.

Consider transmitting and receiving transducers separated by distance ℓ within a turbulent flow. The intervening random fluctuations in sound speed $c(\mathrm{x}, t)$ produce a signal whose pressure amplitude $P(\mathrm{x}, t)$ varies as a function of position x and time t. By convention, the sound speed fluctuations are described by $\mu = (\langle c \rangle - c)/c$, and the acoustic fluctuations by $\chi = \ln(P/\langle P \rangle)$, where the angle brackets indicate ensemble averaging. The space-time correlation function,

$$R_\mu(\mathbf{x}, \mathbf{r}, t, \tau) = \langle \mu(\mathbf{x}, t)\, \mu(\mathbf{x} + \mathbf{r}, t + \tau) \rangle, \qquad (1)$$

provides a simple statistical description of the sound speed field; $\mathbf{r}$ and τ are the spatial and temporal lags, respectively. (If μ is a Gaussian random variable, then this description is also complete, otherwise higher statistical moments need to be specified.) Assuming μ is a stationary random function of space and time, the spectral density of the refractive index fluctuations is defined as the Fourier transform of the correlation function,

$$\varphi_\mu(\mathbf{k}) = \frac{1}{(2\pi)^3} \int_{-\infty}^{\infty} \exp(-i\mathbf{k} \cdot \mathbf{r}) R_\mu(\mathbf{r})\, d\mathbf{r}, \qquad (2)$$

where $\mathbf{k}$ is a wave vector. For isotropic turbulence the vectors $\mathbf{k}$ and $\mathbf{r}$ in (2) can be replaced by their scalar magnitudes k and r, respectively.

Acoustical measurements from a transmitter-receiver pair yield the time-lagged autocorrelation of χ [*Clifford*, 1971],

$$R_\chi(\tau) = \overline{\chi(t)\chi(t + \tau)} = \int_0^{\infty} \cos(2\pi f \tau) G_\chi(f)\, df, \qquad (3)$$

where $G_\chi(f)$ is the temporal spectrum of log-amplitude fluctuations. Here the overbar denotes time averaging which is equivalent to ensemble averaging for an ergodic process and is easier to measure in practice.

Of particular interest to the present analysis is a result which expresses $G_\chi(f)$, the log-amplitude spectrum, in terms of $\varphi_\mu(k)$, the three-dimensional spectral density of the refractive index fluctuations [*Clifford*, 1971],

$$G_\chi(f) = 8\pi^2 k_a^2 \int_0^{\ell} \int_{2\pi f/U_\perp}^{\infty} \left[1 - \cos\left(\frac{k^2 s(\ell - s)}{k_a \ell}\right)\right] \times k\, \varphi_\mu(k) \left[(kU_\perp)^2 - (2\pi f)^2\right]^{-1/2} dk\, ds, \qquad (4)$$

where the acoustic wavenumber $k_a = 2\pi/\lambda_a$, k is a wavenumber associated with turbulence, and $U_\perp$ is the mean flow speed perpendicular to the acoustic path.

This result is valid for spherical waves propagating through weakly scattering homogeneous media, i.e., for $\langle\chi^2\rangle < 0.3$, and for acoustic path lengths much greater than the outer scale of turbulence. It is obtained by assuming that the significant scales, i.e., those in the neighborhood of the first Fresnel zone size, lie in a range where the spectral density of the refractive index fluctuations is isotropic. In addition, Taylor's frozen field hypothesis has been used to relate the spatial and temporal scales of the turbulent flow, as discussed in the introduction.

Kolmogorov Spectrum

The assumption of isotropy is approximately satisfied in the so-called Kolmogorov inertial subrange. Kolmogorov postulated that in high Reynold's number flows there exists a range of wavenumbers, between the energy containing and dissipation ranges, in which the turbulence is locally isotropic and in which the energy spectrum $E(k)$ depends only upon wavenumber k and dissipation rate ε. Dimensional arguments then require that

$$E(k) = A\,\varepsilon^{2/3}\,k^{-5/3}. \tag{5}$$

This approximation is often used to estimate ε [*Gargett et al.*, 1984]. Empirical evidence suggests that $A \approx 1.5$ [*Hinze*, 1975, section 3.5].

Under certain circumstances, sound speed fluctuations behave as advected, passive contaminants which closely follow the turbulent velocity behavior. A similar power law is then predicted for the refractivity spectrum [*Tatarskii*, 1971, section 1.15]

$$\varphi_\mu(k) = 0.033\,C_\mu^2\,k^{-11/3}, \tag{6}$$

where C_μ^2 is the structure parameter that characterizes the strength of refractive index fluctuations. For this particular case, *Clifford* [1971] provides an analytic solution for (4),

$$G_\chi(f) = 2.19\,K\,\Omega^{-8/3}\,\mathrm{Re}\left[1 - H\left(1, \tfrac{-5}{6}, \tfrac{3}{2}, \tfrac{-1}{3}, \tfrac{i\Omega^2}{4}\right) - \tfrac{4}{11}\left(\tfrac{-i\Omega^2}{4}\right)^{4/3}\Gamma\left(\tfrac{-4}{3}\right)H\left(\tfrac{1}{2}, 1, \tfrac{17}{6}, 1, \tfrac{i\Omega^2}{4}\right)\right], \tag{7}$$

where $K = k_a^{2/3}\ell^{7/3}C_\mu^2/U_\perp$, $\Omega = f(2\pi\lambda_a\ell)^{1/2}/U_\perp$, Re indicates the real component of the bracketed expression, $\Gamma(-4/3) \approx 3.05$ is the gamma function, and

$$H(a,b,c,d,z) = \sum_{n=0}^{\infty} \frac{\Gamma(a+n)\Gamma(b+n)\Gamma(c)\Gamma(d)z^n}{\Gamma(a)\Gamma(b)\Gamma(c+n)\Gamma(d+n)n!} \tag{8}$$

is the confluent hypergeometric function. The asymptotic forms of (7) are

$$G_\chi(f) = 0.191\,K\left(1 + 0.119\,\Omega^{4/3}\right) \quad \Omega \ll 1, \tag{9}$$

$$G_\chi(f) = 2.19\,K\,\Omega^{-8/3} \quad \Omega \gg 1. \tag{10}$$

The series in (8) is easily evaluated by noting that the first term of the summation is $h_0 = 1$ and that each successive term can be obtained using the recursive formula

$$h_{n+1} = h_n \frac{(a+n)(b+n)z}{(c+n)(d+n)(n+1)}. \tag{11}$$

However, the convergence of (8) is slow for $\Omega \gg 1$, and the asymptotic form (10) should be used instead.

Equations (4), (6), and (7) describe the effect of random sound speed fluctuations on the underwater scattering of acoustic radiation for a Kolmogorov refractivity spectrum. These results may be readily extended to include the effect of random fluctuations in fluid velocity if C_μ^2 is replaced by the so-called effective spectral structure parameter [*Ostashev*, 1994],

$$C_{\mathrm{eff}}^2 = C_\mu^2 + \frac{11}{6}\frac{C_v^2}{\langle c\rangle^2}. \tag{12}$$

C_v^2 is the velocity structure parameter, and it is related to the dissipation rate by [*Lumley and Panofsky*, 1964, section 2.9]

$$C_v^2 = 1.31A\varepsilon^{2/3} \approx 2\varepsilon^{2/3}. \tag{13}$$

In the event that forward scatter from sound speed fluctuations is negligible relative to that from water-particle velocity fluctuations, the above results afford an estimate of energy dissipation rate based on log-amplitude spectra.

Reciprocal Travel Time Measurements

A second and more direct method of estimating the dissipation rate is provided by two-way acoustical measurements. Reciprocal travel time difference between two points is proportional to the mean along-path velocity component. Let $\mathbf{u}(\mathbf{x}, t)$ be a random velocity field with zero mean and stationary in $\mathbf{x}$ and t which is advected in direction θ relative to measuring baseline $\boldsymbol{\ell}$ by the mean ice–relative flow $\mathbf{U}$. Consider the along-path velocity fluctuations, $u_\theta(\mathbf{x}, t) = \mathbf{u}(\mathbf{x}, t)\cdot\boldsymbol{\ell}/\ell$, where $\ell = |\boldsymbol{\ell}|$. The corresponding spectral density is

$$\varphi_\theta(\mathbf{k}) = \frac{1}{(2\pi)^3}\int_{-\infty}^{\infty} \exp(-i\mathbf{k}\cdot\mathbf{r})\,R_\theta(\mathbf{r})\,d\mathbf{r}, \tag{14}$$

where $R_\theta(\mathbf{r}) = \langle u_\theta(\mathbf{x})\,u_\theta(\mathbf{x}+\mathbf{r})\rangle$. Line averaging over the path vector $\boldsymbol{\ell}$ can be considered as a process which generates a new random velocity field, $\tilde{u}_\theta(\mathbf{x}, t)$. The one-dimensional spectral density of $\tilde{u}_\theta(\mathbf{x}, t)$ is [*Menemenlis*, 1994]

$$\tilde{F}_\theta(k_1) = \frac{1}{2\pi}\int_{-\infty}^{\infty} \exp(-ik_1r_1)\,\tilde{R}_\theta(r_1)\,dr_1 = \iint_{-\infty}^{\infty} \frac{\sin^2(\mathbf{k}\cdot\boldsymbol{\ell}/2)}{(\mathbf{k}\cdot\boldsymbol{\ell}/2)^2}\,\varphi_\theta(\mathbf{k})\,dk_2\,dk_3, \tag{15}$$

where k_1 is the streamwise wavenumber; $k_1 = \mathbf{k} \cdot \mathbf{U}/U$, $U = |\mathbf{U}|$; r_1 is a streamwise displacement; $\tilde{R}_\theta(r_1)$ is the streamwise correlation of $\tilde{u}_\theta$, and k_2, k_3 are the cross-stream wavenumbers. For long measuring baselines compared with the scales of interest, $k_1 \ell \sin\theta \gg 4\pi$, and for the Kolmogorov energy spectrum of (5), it can be shown that [*Menemenlis*, 1993, section 5.2]

$$\tilde{F}_\theta(k_1) \approx \frac{0.84}{\ell} \sin^{5/3}\theta \, A \, \varepsilon^{2/3} \, k_1^{-8/3}. \qquad (16)$$

Equation (16) predicts a $-8/3$ slope for integrated velocity spectra inside the Kolmogorov inertial subrange and provides an estimate of ε given $\tilde{F}_\theta(k_1)$. As before, Taylor's frozen field hypothesis can be used to obtain spatial spectra from the measured frequency spectra. Corrections for anisotropy and the temporal evolution of turbulence were considered by *Menemenlis* [1994], but neither of these two factors is likely to cause errors exceeding 20% when the measuring baseline is approximately perpendicular to the mean relative flow, i.e., when $\theta \sim 90°$. The present result can be combined with forward acoustic scatter measurements in order to separate the contributions of C_μ^2 and C_v^2, the sound speed and water-particle velocity structure parameters, respectively, to the effective structure parameter C_{eff}^2 in (12).

Surface Layer

We now discuss the surface layer approximations which will be used to estimate drag at the ice-ocean interface. Under steady state conditions there often exists a region near the ice where the Reynolds' stress of the fluid $\tau(z)$ does not appreciably change magnitude or direction with depth [*McPhee*, 1986]; that is, $\boldsymbol{\tau}(z) = -\rho\langle w(z)\mathbf{v}(\mathbf{z})\rangle \approx \boldsymbol{\tau}_0$, a constant, ρ is seawater density, $w(z)$ and $\mathbf{v}(z)$ are the vertical and horizontal velocity fluctuations, respectively, and z is the distance from the bottom of the ice. This region is commonly called the surface layer and comprises roughly one tenth of the mixing layer under ice [*McPhee*, 1990]. If in addition to constant stress, the buoyancy fluxes caused by freezing or melting of the ice are negligible, then, on dimensional grounds, the mean velocity gradient is [*Stewart*, 1979]

$$\frac{\partial U(z)}{\partial z} = \frac{u_*}{\kappa z}, \qquad (17)$$

where u_* is the friction velocity, $\tau_0 = |\boldsymbol{\tau}_0| = \rho u_*^2$, and $\kappa \approx 0.4$ is von Kármán's constant. Integrating (17), one finds that the mean velocity profile varies logarithmically with distance from the boundary,

$$U(z) = \frac{u_*}{\kappa} \ln(z/z_0), \qquad (18)$$

where z_0 is a length scale known as the roughness length. It is common to relate the turbulent stress near the surface τ_0 to the mean ice–relative velocity $U(z)$ by the quadratic drag coefficient, $C_D(z)$, so that $\tau_0 = \rho C_D(z) U^2(z)$ and

$$C_D(z) = \frac{u_*^2}{U^2(z)} = \left[\frac{1}{\kappa}\ln(z/z_0)\right]^{-2}. \qquad (19)$$

In the surface layer, storage terms are negligible and the rate of turbulent kinetic energy production by the working of the stress on the mean gradient is approximately balanced by the dissipation rate,

$$\varepsilon(z) = \frac{u_*^3}{\kappa z} = \frac{\tau_0}{\rho}\frac{\partial U(z)}{\partial z}. \qquad (20)$$

Therefore the measurement of dissipation rate ε and mean relative velocity U near the ice can provide estimates of momentum transfer and the drag coefficient. A layer with similar characteristics is also observed in the atmospheric boundary layer above the ice.

Measurements

During the spring of 1989 a horizontal triangular array of acoustical transducers was deployed at the CEAREX oceanography ice camp, 300 km northwest of Spitsbergen. The array had horizontal dimensions of 200 m on a side. It could be raised and lowered to span the upper 20 m of seawater below the ice. The measurements discussed here were obtained while the array was suspended at depths of 20.4 and later 8.4 m relative to the sea level. This corresponds to nominal depths below the ice of 18 and 6 m, respectively, for the observed mean ice thickness of 2.4 m.

For redundancy and to allow recovery of the cross-path horizontal velocity component using amplitude scintillation analysis, each suspended mooring comprised two closely spaced transmitting/receiving transducers. Coded acoustical signals centered at 132 kHz were transmitted between the vertices of the array at a rate of 1 Hz. Two-way travel time and pressure-amplitude time series were recorded. The simultaneous reciprocal travel time measurements along each side of the triangular array provided the basic data set from which velocity, horizontal circulation, and average vorticity were subsequently determined. These measurements are discussed at length by *Menemenlis and Farmer* [1992].

Figure 1 is an acoustic sounding obtained by *Colony* [1989] of the under-ice topography of a portion of the ice field from which the triangular acoustic array was deployed. The locations of the triangular array and of other measurements discussed here are indicated. Figure 1 shows topographic features extending to depths of 10 m. The irregular topography complicates the interpretation of localized boundary layer measurements and indicates the need for the spatial averages that can be provided by the methods discussed in this paper.

By contrast with the open ocean where subsurface bubbles, which are strong acoustic scatterers, are injected to great depths (~12 m) by breaking waves and Langmuir circulation [*Zedel and Farmer*, 1991], the under-ice surface waters provide an acoustically benign environment. Trapped air bubbles remain close to the ice-seawater interface as there are no comparable transport mechanisms. The minimum deployment depth for

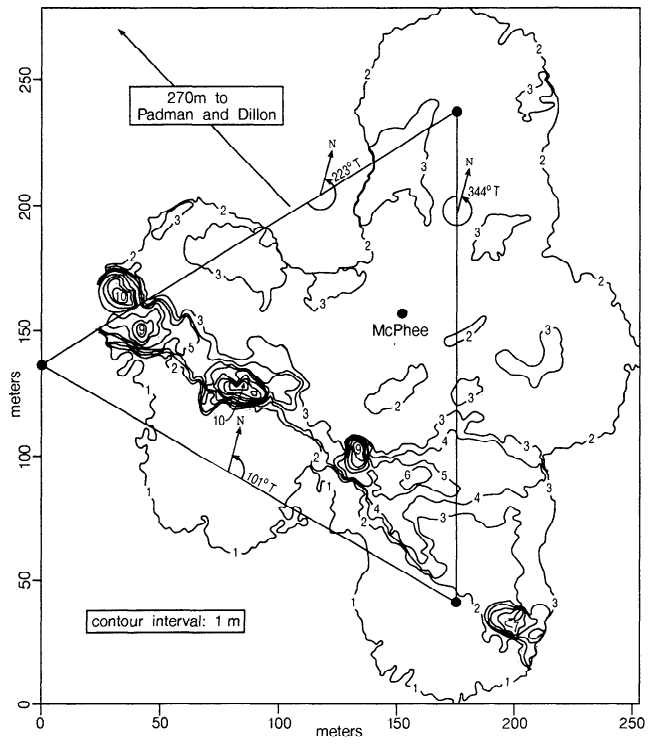

Figure 1. Bottom topography of a portion of the ice field from which was deployed the triangular acoustic array [*Colony*, 1989]. Contour intervals are 1 m. The heights are vertical distance from the ice bottom to the sea level. The locations of the triangular acoustic array and of other measurements discussed are indicated. Deep ice keels that extend to depths of 10 m complicate the interpretation of conventional boundary layer measurements.

the present acoustical experiment was dictated by the need to avoid interference between ice keels and the direct acoustic paths and by the ability of the instrument to resolve the direct and the ice-reflected paths.

The turbulent boundary layer under ice is well mixed and exhibits high Reynold's numbers [*McPhee*, 1990]. Table 1 lists typical values for the mean and the variance of temperature, salinity, and velocity measured by M. G. McPhee (personal communication, 1989) during the experiment. These values were observed at the 6-m depth and correspond to 15-min averaging periods. A simplified empirical equation for sound velocity [*Brekhovskikh and Lysanov*, 1991, section 1.1] is used to estimate the contributions of temperature T, salinity S, and streamwise velocity fluctuations u_1 to the refractive index variance of the flow:

$$\sigma_\mu^2(T) \approx (4.6\,\sigma_T / \langle c \rangle)^2 \sim 10^{-13}, \quad (21)$$

$$\sigma_\mu^2(S) \approx (1.35\,\sigma_S / \langle c \rangle)^2 \sim 10^{-12}, \quad (22)$$

$$\sigma_\mu^2(u_1) \approx (\sigma_u / \langle c \rangle)^2 \sim 10^{-10}. \quad (23)$$

On the basis of these numbers, we expect velocity fine structure to be the main source of forward acoustic scatter and (13) can be used to estimate turbulent kinetic energy dissipation rate from the amplitude scintillation measurements.

Table 1. Mean and Variance of Temperature, Salinity, and Velocity at 6 m Depth

Parameter	Value
$\langle T \rangle$	-1.839°C
$\sigma_T^2 = \langle (T - \langle T \rangle)^2 \rangle$	$(10^{-4}$ °C$)^2$
$\langle S \rangle$	34.12 ‰
$\sigma_S^2 = \langle (S - \langle S \rangle)^2 \rangle$	$(10^{-3}$ ‰$)^2$
U	0.1 m s^{-1}
$\sigma_u^2 = \langle u_1^2 \rangle$	(0.01 m s^{-1})^2

Data represent conditions typical of April 18, 1989, and the averaging period is 15 min (M. G. McPhee, personal communication, 1989). T is temperature, S is salinity, U is the mean ice–relative velocity, and u_1 represents streamwise velocity fluctuation.

Estimates of Energy Dissipation Rate

Figure 2 displays frequency spectra of log-amplitude fluctuations $G_\chi(f)$ for two adjacent horizontal paths at the 6-m depth. The spectra are normalized, so that $\int_0^\infty G_\chi(f)\,df = \langle \chi^2 \rangle$ consistent with (3). The shaded areas enclose the 95% confidence interval. The solid line on Figure 2 is the theoretical spectrum based on (4), (6), (12), and (13) with $\varepsilon = 8 \times 10^{-8}$ W kg^{-1}. Owing to a limitation of the signal recording scheme, which is discussed further later, the accuracy of the scintillation measurements is restricted and white noise

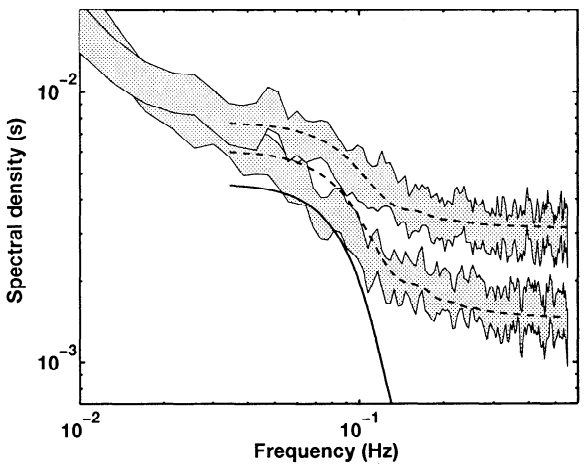

Figure 2. Frequency spectra of log-amplitude fluctuations $G_\chi(f)$ for two adjacent horizontal paths at the 6-m depth, path length $\ell = 211$ m, orientation 344°T. The spectra represent 7-hour averages starting at 1155 UTC on April 18, 1989. During this period the mean ice–relative velocity at that depth was 11 cm s^{-1}, 55°T. The solid line is the theoretical spectrum expected for an isotropic inertial subrange and dissipation rate $\varepsilon = 8 \times 10^{-8}$ W kg^{-1}. The dashed lines are obtained by adding white noise to the theoretical spectrum at levels consistent with those observed at high frequency.

dominates the high-frequency region. Nevertheless, after correction for the observed noise level, the measured log-amplitude spectral levels in the neighborhood of the Fresnel maximum (dashed lines) are consistent with a dissipation of $\varepsilon = 8 \times 10^{-8}$ W kg^{-1}. The correction is based on the assumption of a white noise spectrum at a level consistent with that observed at high frequency which adds incoherently with the spectral level of the signal. At low frequency the assumption of an isotropic inertial subrange does not hold and no agreement between the measurements and the theory is expected.

In contrast to the log-amplitude spectra of Figure 2, the shaded area on Figure 3 encloses the 95% confidence interval of the path-averaged horizontal velocity spectrum $\tilde{F}_\theta(k_1)$ for the same measuring baseline and time interval. Mean along-path velocity was obtained from

$$(\mathbf{U} + \tilde{\mathbf{u}}) \cdot \boldsymbol{\ell}/\ell = \langle c \rangle \, \Delta t/\Sigma t, \tag{24}$$

where Δt and Σt represent the difference and sum of reciprocal travel times, respectively. Taylor's frozen field hypothesis has been used to convert the measured frequency spectrum to a spatial spectrum,

$$\tilde{F}(k_1 = 2\pi f/U) = (U/2\pi)\tilde{F}(f). \tag{25}$$

$\tilde{F}_\theta(k_1)$ is normalized, so that $\int_0^\infty \tilde{F}_\theta(k_1)\, dk_1 = \langle u_\theta^2 \rangle/2$ as per (15).

Before proceeding to use Figure 3 to estimate ε, one needs to understand what is signal and what is noise as was done in considerable detail by *Menemenlis and Farmer* [1992]. Briefly, they determined that the flat part of the spectrum at high frequency is the result of interference from the ice-reflected acoustic arrival and that the spectral peak at $k_1 = 2.5\,\pi$ is caused by relative motion between the transducers during reciprocal transmissions. Mooring motion error drops off rapidly at frequencies higher than the mechanical resonance frequency of the suspended moorings but remains relatively flat at lower frequencies after an initial drop by a factor of 4 from the resonance peak. The log-amplitude spectra of Figure 2 are, to a large extent, insensitive to mooring motion, but their accuracy is limited by interference from the ice-reflected arrivals. In future experiments both noise sources could be reduced by increasing acoustic signal discrimination between the direct and ice-reflected paths and by using the one-way travel time measurements to predict and correct relative mooring motion during each reciprocal transmission.

A line of slope $-8/3$ is fitted to the wavenumber range corresponding to turbulent eddy scales $\pi/k_1 = 2$–20 m (solid line). Smaller scales cannot be used for the analysis because, as discussed, they are contaminated by mooring motion. The proximity of the ice (6 m) limits the validity of the isotropic assumption at these scales. However, observations in turbulent flows [*Gargett et al.*, 1984] have shown uniform spectral slopes of $-5/3$ extending beyond the inertial subrange with the correct Kolmogorov constant A in (5), and we therefore evaluate the dissipation ε on this basis. Equation (16) yields a mean value of $\varepsilon \approx 8 \times 10^{-8}$ W kg^{-1}. Although the range of scales at which the log-amplitude and the path-averaged velocity measurements can be compared is limited, both measurements produce consistent results.

In Figure 4 we compare the value of mean dissipation rate obtained using scintillation analysis with profiles obtained by *Padman and Dillon* [1991] using a shear microstructure profiler. The shear microstructure pro-

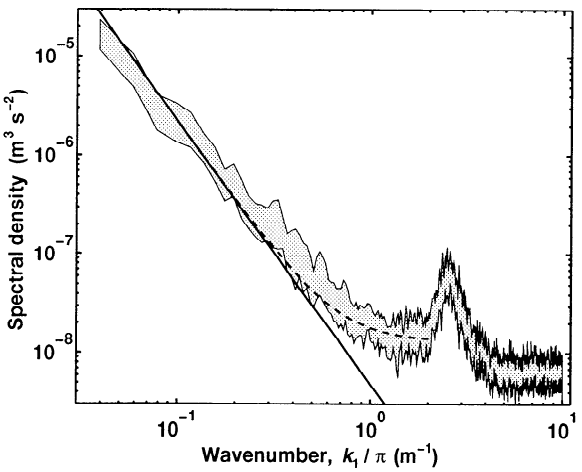

Figure 3. Spectral density of path-averaged horizontal velocity $\tilde{F}_\theta(k_1)$ at the 6-m depth for the same path and time interval as Figure 2. The solid line is proportional to $k_1^{-8/3}$ at the level expected for an isotropic inertial subrange and dissipation rate $\varepsilon = 8 \times 10^{-8}$ W kg^{-1}. As discussed in the text, the spectral peak at $k_1 = 2.5\,\pi$ is caused by relative motion between the two suspended moorings. The dashed line is a correction to the theoretical spectrum for mooring motion noise.

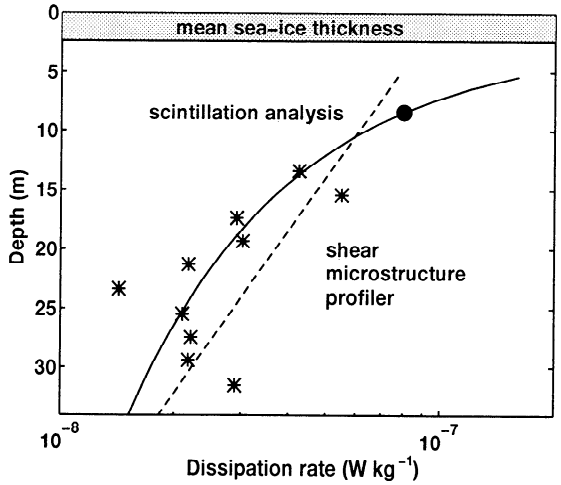

Figure 4. Dissipation rate as a function of depth from scintillation analysis (solid circle), and from shear microstructure profiles (stars) [*Padman and Dillon*, 1991]. The data points are 7-hour averages starting at 1155 UTC on April 18, 1989. The microstructure profiler data are also averaged over 2-m depth bins. The dashed line is an exponential fit to the profiler estimates of ε, and the solid line is an estimate of $\varepsilon(z)$ based on scintillation analysis and the assumption of a logarithmic surface layer extending out to 35 m depth.

filer measurements are only reliable below about 12 m because of instrument vibration following release. To determine the contribution to the depth-integrated dissipation rate,

$$\varepsilon_{\text{int}} = \int_0^D \varepsilon(z)\, dz, \tag{26}$$

from the unresolved surface layer, 0 m $< z <$ 12 m, *Padman and Dillon* [1991] assumed that the dissipation rate decays exponentially,

$$\varepsilon(z) = \alpha \exp(-\beta z), \tag{27}$$

consistent with the decay rate found in the resolved portion of the profile, 12 m $< z < D$, where D is the mixed layer depth. The dashed line on Figure 4 is an exponential fit to the profiler dissipation data. The solid line is an estimate of dissipation rate obtained from scintillation measurements using the constant stress surface layer approximation of (20).

Figure 5 is an 11-day time series of turbulent kinetic energy dissipation rate obtained using reciprocal travel time measurements at the 18-m depth. Each point on Figure 5 is obtained from a 12-hour average spectrum of horizontally integrated velocity measurements. At this depth, contamination of the measurements from mooring motion occurred at a lower frequency than at the 6-m depth, and we had to restrict the analysis to the wavenumber range corresponding to turbulent eddy scales π/k_1 =10–25 m. As before, it is assumed that the $-5/3$ region extends outside the isotropic inertial subrange for horizontal velocity fluctuations, and (16) is used to estimate ε. The acoustical measurements of dissipation are compared with concurrent estimates obtained with the microstructure profiler by *Padman and Dillon* [1991] and with turbulence clusters by *McPhee* [1992]. From (20) the dissipation rate is expected to scale roughly as the cube of the mean ice–relative current speed, which is also displayed on Figure 5. The qualitative agreement between the different types of measurements is encouraging, given the respective limitations of the instruments used; it is a demanding test of the several assumptions made in order to arrive at the above results.

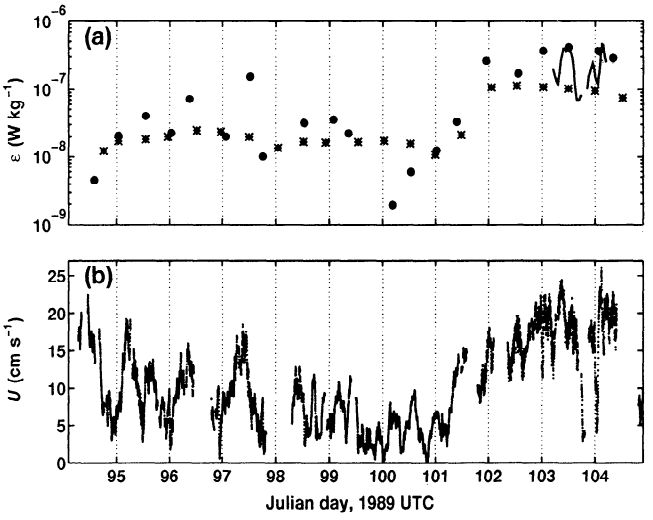

Figure 5. (a) Comparison of estimates of dissipation rate from a microstructure profiler (stars) [*Padman and Dillon*, 1991], turbulence clusters (solid line) [*McPhee*, 1992], and the acoustical current meter (solid circles) at the 18-m depth. (b) Ice–relative current speed at 18 m depth.

Local Ice Strain

The particular configuration of the acoustic array provides a direct measurement of circulation around the ice keels enclosed by the acoustic paths:

$$\Gamma = \oint \mathbf{u} \cdot \mathrm{ds} = \frac{\langle c \rangle^2}{2} \Delta t, \tag{28}$$

where Δt is the reciprocal travel time difference around the triangular array and $\langle c \rangle$ is the mean sound speed. Typical values of circulation measured at the 6-m depth during the experiment were of order 10 m^2 s^{-1} for mean ice–relative velocity of 0.1 m s^{-1} [*Menemenlis and Farmer*, 1992]. R. W. Stewart (personal communication, 1993) suggested that these measurements could be used to estimate the "lift" force due to flow around the ice keels. Here the lift force acts on the ice keels in a horizontal direction perpendicular to the mean flow, in a way similar to that of wind flowing around a sail. The lift force per unit length L is proportional to circulation Γ and mean flow speed U [*Kundu*, 1990, section 6.10]:

$$L = \rho \Gamma U, \tag{29}$$

where ρ is seawater density. Figure 1 indicates that the acoustic array encloses a pressure ridge keel with characteristic depth of order 10 m. Therefore the lift force exerted on the ice keel is of order 10^4 N for typical values of Γ and U measured during CEAREX. The magnitude of this force is significant when compared to the drag due to turbulent stress on the region spanned by the acoustic array, $\tau_0 A_T \approx 625$ N, where $\tau_0 \approx 0.03$ N m^{-2} is the value derived earlier and $A_T = 18,300$ m^2 is the area enclosed by the array. However on the one hand, drag due to turbulent stress is more or less uniform and unidirectional, and it adds up over large regions. On the other hand, the magnitude of the lift force depends on the depth and shape of each ice keel, and it is directed either to the right or to the left of the mean ice–relative flow. Therefore on average the effect of the lift force on the ice is negligible. Nevertheless, this type of ice-flow interaction may be at least in part responsible for observed background noise in the strain measurements obtained at the ice camp [*Williams et al.*, 1990; *Czipott et al.*, 1991]. For example, a force of 10^4 N applied across a vertical section of the ice of area 100 m^2 would cause a compressional strain of 10^{-8}, given the typical value of 10^{10} Pa for the elastic modulus of sea ice [*Tabata*, 1958].

Discussion

We have obtained an estimate of energy dissipation rate at the 6-m depth, $\epsilon = 8 \times 10^{-8}$ W kg^{-1}, for a 7-hour period during which the mean ice–relative velocity at that depth was 11 cm s^{-1}, with a standard deviation of 1.2 cm s^{-1}. This interval was selected for analysis because the relatively constant flow speed and direction simplifies the interpretation of the data. Given an overturning timescale of order 1 hour [*Padman and Dillon*, 1991], it was assumed that the turbulent field was sufficiently well developed and stationary to satisfy the assumptions of steady state and statistical equilibrium. It is now further assumed that the surface layer approximations discussed earlier are also satisfied at the 6-m depth. From (18), (19), and (20) we estimate a turbulent stress near the ice-water interface of $\tau_0 = 0.03$ N m^{-2}, a drag coefficient $C_D(6\text{ m}) = 0.003$, and a roughness length $z_0 = 0.003$ m. These values are consistent with previous measurements under multiyear pack ice [*McPhee*, 1990] of $0.002 < C_D(6\text{ m}) < 0.01$ and $0.002\text{ m} < z_0 < 0.1$ m.

Under steady state conditions the atmospheric stress exerted on the ice is balanced by drag at the ice-water interface, a term normal to the velocity of the ice due to planetary rotation and the gradient of internal ice stress (including loads transmitted from any nearby land masses) [*McPhee*, 1990]. For a first-order analysis we neglect internal ice stress and the Coriolis term and assume the magnitude of atmospheric stress is roughly balanced by the magnitude of oceanic stress near the ice. During the dissipation measurements a steady northerly wind, $U_a(2.82\text{ m}) = 7$ m s^{-1}, was recorded [*Guest and Davidson*, 1989]. For the measured atmospheric conditions of -17°C, 1.03 bar, and 72% relative humidity, the density of air above the ice is 1.4 kg m^{-3} (see *Weast* [1982], density of moist air). We use the surface layer approximation (19) to estimate the drag coefficient $C_a(10\text{ m}) = 4.3 \times 10^{-4}$ and roughness length $z_a = 4.7 \times 10^{-8}$ m associated with momentum transfer between the atmosphere and the ice. These estimates are much lower than previous estimates over multiyear ice [*Brown*, 1990; *Guest and Davidson*, 1991] and than concurrent atmospheric estimates of $C_a(10\text{ m}) \approx 2.2 \times 10^{-3}$ and $z_a \approx 2.0 \times 10^{-3}$ m (P. S. Guest, personal communication, 1989). Therefore it is concluded that the internal stress gradient of the ice cannot be neglected.

Padman et al. [1992] point out that diurnal tidal currents in the vicinity of the Yermak Plateau are enhanced by the plateau topography. These tidal currents cause stress divergence at the base of the ice which greatly exceeds the typical divergence of the surface wind stress. This mechanism is thought to be responsible for the anomalously deep mixing layer observed under the ice camp (~100 m) and for introducing the large internal stress gradients inferred above.

The kinetic energy flux from the ice to the ocean is proportional to ρu_*^3, where ρ is seawater density and u_* is friction velocity as in (20). *Padman and Dillon* [1991] estimated the proportionality constant by assuming that all kinetic energy input at the surface is dissipated locally and that buoyancy effects are negligible. They estimate that the depth-integrated dissipation rate is

$$\epsilon_{\text{int}} \approx 2.4\,\rho u_*^3. \tag{30}$$

This may be compared to proportionality constants of 4 and 6 obtained from open ocean studies by *Oakey and Elliott* [1982] and *Dewey and Moum* [1990], respectively. The lower value in the Arctic may, in part, result from the unique mechanism of momentum transfer between the ice and the mixed layer and from the absence of surface waves or direct interaction between the atmosphere and the ocean.

Figure 4 suggests that another possible cause for the low proportionality constant may be that energy dissipation rate is underestimated by profiler data because the unresolved near-surface dissipation rates are higher than approximation (27) made by *Padman and Dillon* [1991]. Specifically, if (20) instead of (27) (i.e., the solid line instead of the dashed line in Figure 4) is used to estimate ϵ in the unresolved near-surface waters (0.1 to 12 m from the bottom of the ice), then an additional 1.5×10^{-6} m^3 s^{-3} would be obtained, which would double the proportionality constant in (30) and bring it more in line with previous estimates.

Conclusions

Though a limitation of the signal-recording scheme restricts the accuracy of the scintillation measurements, the present results demonstrate the usefulness of amplitude scintillation analysis and reciprocal travel time measurements for the study of the Arctic boundary layer. The simultaneous availability of both types of measurements makes it possible to separate the contributions of sound speed and water-particle velocity fine structure to forward acoustic scatter. The observed log-amplitude variance measured during the Arctic experiment is almost exclusively caused by velocity fine structure. Therefore scintillation analysis can be used to estimate turbulent kinetic energy dissipation rate and provides an independent check on the value obtained using reciprocal travel time measurements.

The comparison of dissipation estimates in Figures 4 and 5 is a check on the assumptions made for arriving at estimates of ϵ. The greatest uncertainty for the reciprocal travel time method lies in the extension of the $k_1^{-8/3}$ range outside the Kolmogorov inertial subrange. The rough agreement between the four types of measurements is encouraging. Minor modifications to the acoustic instrumentation could provide the full spectrum and improve the results substantially.

The principal advantage of the methods described in this paper is the ability to obtain measurements which are averages over long measuring baselines, thus overcoming some of the limitations of conventional point measurements in studying intermittent and localized turbulence events.

Acknowledgments. We thank R. Colony, T. M. Dillon, M. G. McPhee, and L. Padman for making their data available. We are indebted to D. DiIorio, M. G. McPhee, R. W. Stewart, and two anonymous reviewers for helpful comments and suggestions. The work was supported by the U.S. Office of Naval Research under a program directed by T. B. Curtin, and the first author was funded by scholarships from the Natural Sciences and Engineering Research Council of Canada and the Science Council of British Columbia.

References

Brekhovskikh, L., and Y. Lysanov, *Fundamentals of Ocean Acoustics*, 2nd ed., Springer-Verlag, New York, 1991.

Brown, R. A., Meteorology, in *Polar Oceanography, Part A: Physical Sciences*, edited by W. O. Smith, Jr., chap. 1, pp. 1–46, Academic, San Diego, Calif., 1990.

Clifford, S. F., Temporal-frequency spectra for a spherical wave propagating through atmospheric turbulence, *J. Opt. Soc. Am.*, *61*(10), 1285–1292, 1971.

Colony, R., Measurement of bottom topography of the ice at the CEAREX oceanography camp, Appl. Phys. Lab., Seattle, Wash., 1989.

Czipott, P. V., M. D. Levine, C. A. Paulson, D. Menemenlis, D. M. Farmer, and R. G. Williams, Ice flexure forced by internal wave packets in the Arctic Ocean, *Science*, *254*(5033), 832–835, 1991.

Dewey, R. K., and J. N. Moum, Enhancement of fronts by vertical mixing, *J. Geophys. Res.*, *95*(C6), 9433–9445, 1990.

DiIorio, D., and D. M. Farmer, Path-averaged turbulent dissipation measurements using high-frequency acoustical scintillation analysis, *J. Acoust. Soc. Am.*, *96*(2), 1056–1069, 1994.

Farmer, D. M., S. F. Clifford, and J. A. Verrall, Scintillation structure of a turbulent tidal flow, *J. Geophys. Res.*, *92*(C5), 5369–5382, 1987.

Flatté, S. M., Wave propagation through random media: Contributions from ocean acoustics, *Proc. IEEE*, *71*(11), 1267–1294, 1983.

Gargett, A. E., T. R. Osborn, and P. W. Nasmyth, Local isotropy and the decay of turbulence in a stratified fluid, *J. Fluid Mech.*, *144*, 231–280, 1984.

Guest, P. S., and K. L. Davidson, CEAREX/"O" and "A" Camp meteorology atlas, *Data Rep. NPS-63-89-007*, Nav. Postgrad. School, Monterey, Calif., 1989.

Guest, P. S., and K. L. Davidson, The aerodynamic roughness of different types of sea ice, *J. Geophys. Res.*, *96*(C3), 4709–4721, 1991.

Hinze, J. O., *Turbulence*, 2nd ed., McGraw-Hill, New York, 1975.

Kundu, P. K., *Fluid Mechanics*. Academic, San Diego, Calif., 1990.

Langleben, M. P., Water drag coefficient of first-year ice, *J. Geophys. Res.*, *87*(C1), 573–578, 1982.

Lee, R. W., and J. C. Harp, Weak scattering in random media, with applications to remote probing, *Proc. IEEE*, *57*(4), 375–406, 1969.

Lumley, J. L., and H. A. Panofsky, *The Structure of Atmospheric Turbulence*. John Wiley, New York, 1964.

McPhee, M. G., The upper ocean, in *The Geophysics of Sea Ice*, edited by N. Untersteiner, chap. 4, pp. 339–394, Plenum, New York, 1986.

McPhee, M. G., Small-scale processes, in *Polar Oceanography, Part A: Physical Sciences*, edited by J. Walker O. Smith, chap. 6, pp. 287–334, Academic, San Diego, Calif., 1990.

McPhee, M. G., Turbulent heat flux in the upper ocean under sea ice, *J. Geophys. Res.*, *97*(C4), 5365–5379, 1992.

Menemenlis, D., Acoustical measurement of velocity, vorticity and turbulence in the arctic boundary layer beneath ice, Ph.D. thesis, Univ. of Victoria, Victoria, B.C., 1993.

Menemenlis, D., Line-averaged measurement of velocity fine structure in the ocean using acoustical reciprocal transmission, *Int. J. Remote Sens.*, *15*(2), 267–281, 1994.

Menemenlis, D., and D. M. Farmer, Acoustical measurement of current and vorticity beneath ice, *J. Atmos. Oceanic Technol.*, *9*(6), 827–849, 1992.

Oakey, N. S., and J. A. Elliott, Dissipation within the surface mixed layer, *J. Phys. Oceanogr.*, *12*, 171–185, 1982.

Ostashev, V. E., Sound propagation and scattering in media with random inhomogeneities of sound speed, density and medium velocity, *Waves Random Media*, *4*, 403–428, 1994.

Padman, L., and T. M. Dillon, Turbulent mixing near the Yermak Plateau during the coordinated eastern Arctic experiment, *J. Geophys. Res.*, *96*(C3), 4769–4782, 1991.

Padman, L., A. J. Plueddemann, R. D. Muench, and R. Pinkel, Diurnal tides near the Yermak Plateau, *J. Geophys. Res.*, *97*(C8), 12,639–12,652, 1992.

Shirasawa, K., Water stress and ocean current measurements under first-year sea ice in the Canadian Arctic, *J. Geophys. Res.*, *91*(C12), 14,305–14,316, 1986.

Stewart, R. W., The atmospheric boundary layer, *Third IMO Lect. 523*, World Meteorol. Organ., Geneva, 1979.

Tabata, T., Studies on visco-elastic properties of sea ice, in *Arctic Sea Ice*, pp. 139–147. Natl. Acad. of Sci. and Natl. Res. Counc., Washington, D.C., 1958.

Tatarskii, V. I., *The Effects of the Turbulent Atmosphere on Wave Propagation*. Israel Program for Scientific Translations, Jerusalem, 1971.

Tatarskii, V. I., Review of scintillation phenomena, in *Wave Propagation in Random Media (Scintillation)*, edited by V. I. Tatarskii, A. Ishimaru, and V. U. Zavorotny, pp. 2–15, SPIE – The Int. Soc. for Opt. Eng., Bellingham, Wash., 1993.

Weast, R. C. (Ed.), *CRC Handbook of Chemistry and Physics*, 62 ed., CRC Press, Boca Raton, Fla., 1982.

Williams, R. G., N. R. Davis, and S. C. Moore, The coordinated eastern Arctic experiment: SPRI sea-ice studies, *Polar Rec.*, *26*(158), 203–210, 1990.

Yamazaki, H., R. G. Lueck, and T. Osborn, A comparison of turbulence data from a submarine and a vertical profiler, *J. Phys. Oceanogr.*, *20*, 1778–1786, 1990.

Zedel, L., and D. Farmer, Organized structures in subsurface bubble clouds: Langmuir circulation in the open ocean, *J. Geophys. Res.*, *96*(C5), 8889–8900, 1991.

D. M. Farmer, Ocean Physics, Institute of Ocean Sciences, Post Office Box 6000, Sidney, British Columbia, Canada V8L 4B2. (e-mail: dmf@ios.bc.ca)

D. Menemenlis, Earth, Atmospheric, and Planetary Sciences, Massachusetts Institute of Technology, Building 54 Room 1511, Cambridge, MA 02139.
(e-mail: dimitri@sea.mit.edu)

(Received July 1, 1994; revised March 16, 1995;
accepted March 23, 1995.)